# Superplumes from the core-mantle boundary to the base of the lithosphere

Barbara Romanowicz[1*], Yuancheng Gung[1]

[1*]Seismological Laboratory, University of California, Berkeley

215, McCone Hall, Berkeley, CA 94720, USA

*To whom correspondence should be addressed; Email:barbara@seismo.berkeley.edu

submitted to *Science* January 22, 2002

---

**Three-dimensional modelling of upper-mantle anelastic structure reveals that upwellings associated with the two large "superplumes", imaged by seismic elastic tomography at the base of the mantle, persist through the upper-mantle transition zone, and are deflected horizontally beneath the lithosphere. This provides a simple explanation for the unique transverse isotropy in the central Pacific. We infer that the two superplumes may play a major and stable role in supplying heat and horizontal flow to the low viscosity asthenospheric channel, lubricating plate motions. We suggest that more heat may be carried through the core-mantle boundary than is accounted for by hot-spot fluxes alone. Also, the direct geographic relation of the two main upwellings and most hotspots may shed some light on the distribution of geochemical signatures in ocean island basalts.**

Global seismic tomography aims at improving our understanding of mantle dynamics by providing constraints on 3D temperature and composition, using elastic velocities as proxies. Much progress has been made in recent years in resolving increasingly finer details in the 3D distribution of elastic velocities from the inversion of seismic phase and travel time data *(1-2)*. In particular, regions of faster than average velocity, associated with subduction around the Pacific rim, have revealed a variety of behaviors of lithospheric slabs in the transition zone, some stagnant around the 670km discontinuity, while others appear to penetrate into the lower mantle to depths in excess of 1500 km *(3)*. These results are in good agreement with geodynamic models in which the cold and dense downgoing slabs play a driving role in global mantle circulation heated primarily from within *(4)*. On the other hand, the detailed morphology and role of upwellings, as manifested by two prominent zones of significantly lower than average velocity, commonly referred to as "superplumes", in the lowermost mantle, is less clear. Their location, under the south-central Pacific and under Africa, correlates with the global distribution of hotspots, as well as two major geoid highs *(5)*. Recent tomographic S velocity models suggest that they rise high above the core-mantle boundary (CMB)*(2,6)*. However, finer scale resolution is still lacking. In particular, velocity tomography in the transition zone correlates well with slabs, but not so well with hotspot distribution or the residual geoid, except at degree 6 *(7)*. This could be due to a combination of factors: (1) elastic velocities are sensitive both to composition and temperature; (2) the effect of temperature on velocities decreases with increasing pressure*(8)*; wavefront healing effects make it difficult to accurately image low velocity bodies *(9)*. Finally, hotspots could have a shallow origin, independent of the lower mantle superplumes *(10)*.

To obtain additional constraints on rising, hotter than average currents, we turn to the amplitudes of seismic waves, which are sensitive to 3D anelastic structure. Owing to the exponential dependence on temperature of attenuation (or its inverse, the quality factor Q *(11)*), we expect anelastic tomography to highlight hotter than average regions

better than standard elastic tomographic approaches.

There have been few attempts at mapping mantle 3D attenuation structure. Unlike travel time and phase observations, which, in general, can be successfully interpreted in the framework of linear ray theory, amplitudes are affected not only by anelastic structure, but at least equally strongly by the non-linear effects of wave propagation through the 3D elastic medium, which causes focusing and scattering of energy *(12)*. Because the lateral gradients of elastic structure are not sufficiently well constrained at present to allow the accurate removal of elastic effects, the resulting contamination of amplitude data can be severe. Particular care must therefore be taken in data selection and methodology in order to extract the intrinsic attenuation signal.

Previous studies of lateral variations of Q in the upper mantle have noted low Q regions associated with ridges *(13)* and back arcs *(14)*, and suggested the existence of a degree 2 in attenuation *(12,15)*. However, on the global scale, 3D mantle Q models have remained largely qualitative *(16)*.

We have developed a waveform tomographic inversion method, originally aimed at constructing global 3D elastic models of the whole mantle*(2,17)*, which now has been extended to iteratively solve for elastic and anelastic structure in the upper mantle, using three-component waveform data of fundamental and higher mode surface waves *(18)*. While we do not directly account for elastic effects in the amplitudes, which currently limits the lateral resolution of our Q models to $lmax = 8$, where $lmax$ is the maximum degree in a horizontal spherical harmonics parametrization *(21)*, strict data selection criteria are designed to reject data most strongly contaminated by focusing *(22)*. The first step (elastic inversion) allows us to align the phases in our waveforms, and we do so separately for SV sensitive (vertical and longitudinal component) and SH sensitive (transverse component) data, to account for significant anisotropy in the uppermost mantle*(23,24)*. In the second step, the Q model, $QRLW8$, is derived using all three component data *(25)*.

Figure 1 shows map views of model $QRLW8$ at representative depths. In the top 250 km of the mantle, correlation of high Q regions with shields is seen systematically in North and South America, Eurasia, Australia and Antarctica, whereas mid-ocean ridges in the Pacific, Atlantic and Indian Ocean exhibit generally low Q values, as do western Pacific back-arc regions. This is similar to what is observed in elastic velocity models, with regions of high/low velocity correlated with regions of high/low Q. A notable exception is an elongated zone of low Q in the central Pacific, extending from south of the equator to Hawaii, not seen in $SH$ velocity models *(2,17)* at these depths. Below 250 km, this tectonics-related Q distribution is gradually replaced by a simpler pattern, with two strong low Q minima centered in the southern Pacific and under Africa, throughout the upper mantle transition-zone. At depths greater than 400 km, a majority of hotspots are located above regions of low Q .

A remarkable feature of model $QRLW8$ is that the low Q regions in the transition zone coincide in location with the minima in elastic velocity associated with the two superplumes in the lowermost mantle. Correlation between Q in the transition zone and velocity in the last 500 km of the mantle is particularly strong at degree 2 (Figure 2), but persist at shorter wavelengths. Cross-sections in the Pacific (Figure 3a) and under Africa (Figure 3b) comparing upper mantle Q with lower mantle velocity distributions, all filtered to the same $lmax = 8$, emphasize the vertical correspondence of the lowermost mantle superplumes with transition zone low Q zones. Because our Q model does not extend to the lower mantle, and the low velocity zones are only expressed faintly in the upper half of the lower mantle, where they appear to be narrower and have a contorted shape, it is not possible to determine whether the superplumes are simply continuous across the 670 km discontinuity, or whether they induce rising hot currents in the upper mantle through thermal coupling processes. However, our results show that the superplumes must carry significant energy across the lower mantle to create coherent upwelling flow in the upper mantle transition zone. In contrast, ridges are shallow low Q features, mostly confined to

the upper 200 km of the mantle.

The cross-sections in Figure 3 also show that the low Q zones in the transition zone connect with shallower ones whose positions are significantly shifted horizontally, suggesting that the upwelling, plume related flow is deflected horizontally below the cold lithosphere, towards the Indian and Atlantic mid-ocean ridges under Africa, and in the Pacific, towards the East Pacific rise and the center of the Pacific plate. In the latter case, the flow is impeded on the west side by the presence of the Fiji-Tonga subduction zone. This deflection occurs at greater depths under the thicker continental lithosphere ($\sim 350km$, Figure 3b) than under the oceanic one ($\sim 200km$, Figure 3a).

This change in direction of the upwelling flow is supported by the presence of significant anisotropy (transverse isotropy), as seen by comparing $V_{SH} - V_{SV}$ cross-sections with those of Q (Figure 3ab). Zones of $V_{SH}$ faster than $V_{SV}$ correlate with zones where the deeper low Q channels spread horizontally towards the uppermost mantle ones. The existence of horizontal flow related to the spreading of upwelling flow beneath the lithosphere provides a simple explanation for the existence of strong transverse isotropy in the central Pacific, in particular under Hawaii, with $SH$ velocity greater than $SV$ velocity *(24)*, which may not require invoking complex microscopic material properties *(28)*. Also, azimuthal anisotropy (not shown), which consistently shows fast directions aligned perpendicular to the ridge in the vicinity of the East Pacific Rise, displays a more complex pattern in the central Pacific*(23,29)*. This is consistent with the spreading of upwelling flow associated with the superplumes into the asthenospheric low viscosity channel, which perturbs the ridge-perpendicular lithospheric drag flow, and creates a complex horizontal flow pattern in the central Pacific. The case of Hawaii is particularly intriguing. The "hot" anomaly associated with this hot spot, as seen in the Q models (Figure 3a), is primarily expressed at shallow depth (less than 300 km), and appears to be "fed" from the more southerly upwelling by horizontal flow beneath the lithosphere.

These results suggest a potentially important role for superplumes in the dynamics

of the mantle: significant "action" may well take place in the shallow mantle, where hot material injected by the superplumes lowers the viscosity of the asthenosphere *(30)*, lubricating the motion of the lithospheric plates. In particular, this would allow for efficient slab pull in the Pacific, and contribute to heating of the continental lithosphere under Africa*(31)* . Most hotspots are directly derived from the two main upwellings. Exceptions appear to be hotspots in north America and perhaps Iceland, whose signature in the Q models is lost below 400 km, and whose deep or shallow origin has been the subject of vigorous debate*(6)(32)*. The relation of the position of different hotspots with respect to the centers of the major upwellings may provide clues on their distinctive geochemical signatures *(33)*, particularly in view of the noted correlation of the lower mantle superplumes with the Dupal anomaly *(34)*.

Previous suggestions on the relation of major flood basalts to the two superplumes *(35)* and the stability of absolute hot spot locations *(36)*, combined with the results of the present study indicate that the two major lower mantle plumes may not be mere instabilities in the mantle convective system. In particular, the estimate of $\pm 10\%$ heat from the core carried by plumes *(37)* may need to be revised to account not only for hotspot flux, but also for heat carried horizontally in the asthenosphere and eventually contributed to the ridge system.

## References and Notes


1. Grand, S., R. van der Hilst and S. Widiyantoro, *GSA Today* **7**,4,1 (1997); Masters G., Johnson, S., Laske, G. and Bolton, B., *Philos. Trans. R. Soc. Lond. A* **354**, 1,385 (1996); Gu, Y. J., A.. M. Dziewonski, W.-J. Su, and G. Ekström, *J. Geophys. Res.* **106**, 11169 (2001).

2. Mégnin, C. and B. Romanowicz, *Geophys. J. Inter.* **143**, 709 (2000).

3. Van der Hilst, R.D., S. Widiyantoro and E. R. Engdahl, *Nature* **386**, 578 (1997); Fukao, Y., S. Widiyantoro and M. Obayashi, *Rev. of Geophys.* **39**, 291 (2001).

4. Bercovici, D., Y. Ricard and M. A. Richards, *AGU Geophys. Monogr.* **121**, 5 (2000).

5. Hager, B., R.W. Clayton, M. A. Richards, R. P. Comer and A. M. Dziewonski, *Nature* **313**, 541 (1985).

6. Ritsema, J. , H. van Heijst and J. Woodhouse, *Science* **286**, 1925-1928, 1999.

7. Richards, M., B. H. Hager and N. H. Sleep, *J. Geophys. Res.***93**, 7690 (1988).

8. Karato, S. I. *Geophys. Res. Lett* **20**, 1623 (1993).

9. Nolet, G. and F. A. Dahlen, *J. Geophys. Res.* **105**, 19,043 (2000).

10. Anderson, D. L., *Science* , 2016 (2001).

11. Jackson, I., *in Mineral Physics and Seismic Tomography AGU geophys. Monograph Ser., S. Karato Ed*, 265 (2000); Minster, J. B. and D. L. Anderson, *Philos. Trans. R. Soc. London A*, **299**, 319 (1981); Karato, S. I., *Pageoph.* **153**, 239 (1998);

12. Romanowicz, B., *J. Geophys. Res.* **95**, 11,051 (1990).

13. Ding, C.-Y. and S.P. Grand, *J. Geophys. Res.* **98**, 1973 (1993); Romanowicz, B. *J. Geophys. Res.* **100**, 12,375 (1995); Billien, M., J.J. Lévêque and J. Trampert, *Geophys. Res. Lett.* **27** , 3619 (2000); Reid, F. J. L., J. H. Woodhouse and H. H. van Heist, *Geophys. J. Int.* **145,** 695 (2001).

14. Roth, E. G., D. Wiens, L. M. Dorman, J. Hildebrand and S. Webb, *J. Geophys. Res.* **104** 4795 (1999).

15. Suda, N., N. Shibata abd Y, Fukao, *Geophys. Res. Lett.* **18**, 1119 (1991); Durek, J.

J. , M. H. Ritzwoller and J.H. Woodhouse, *Geophys. J. Int.* **114**, 249 (1993).

16. Due to accumulation of numerous regional surface wave and Lg wave data, the lateral variations of Q in the crust are somewhat better constrained, and show correlation with tectonics [ Mitchell, B. J., *Rev. Geophys. Space Phys.* **33**, 441 (1995)].

17. Li, X.D. and B. Romanowicz, *J. Geophys. Res.* **101** 22,245 (1996).

18. The inversion involves comparison of observed waveforms, of surface waves and body waves, with synthetics computed using normal mode theory. It proceeds in two steps *(19)*. In the first step, waveform phases are aligned by constructing 3D elastic models of the mantle separately for $SH$ (transverse component) and $SV$ (vertical and longitudinal component) using the coupled-mode approach developed for $SH$ models *(17)*. In the second step, we invert for $Q$, starting from a spherically symmetric reference $Q$ model and the 3D velocity models obtained in the previous step. For this specific study, focused on the retrieval of $Q$ structure, velocity models are parametrized up to maximum spherical harmonics degree $smax = 16$ horizontally, and using 16 B-splines vertically (throughout the mantle). The $Q$ models have $smax = 8$ in the horizontal direction and 7 B-splines in the vertical direction, utilize only fundamental and higher mode surface wave packets and are restricted to the upper mantle. Crustal corrections utilize model Crust5.1 *(20)* for velocities. We invert only for Q structure below 80 km, correcting for shallow structure using information on Moho variations from Crust5.1.

19. Gung, Y. C., B. Romanowicz and S. I. Karato, *EOS Trans. AGU* **82**, 1268 (2001).

20. Mooney, W. D., G. Masters and G. Laske, *J. Geophys. Res.* **103**, 727 (1998).

21. Selby, N. D. and J. H. Woodhouse, *Geophys. J. Int* **142**, 933-940 (2000).

22. Because we do not explicitely correct for focusing and scattering effects due to wave propagation in the complex 3D elastic earth, it is particularly important to inspect the waveforms, once the phases are aligned, before inversion for $Q$ structure. Comparison of synthetic and observed waveforms based on criteria involving correlation coefficients and variance reduction results in the rejection of wavepackets that are strongly contaminated

by effects other than anelastic structure. While some selection already occurs in the first step (elastic inversion), it is most important in the second step, where only $\sim$ 50% of the wavepackets used in the velocity inversion are kept for Q inversion. The comparison of models obtained separately from vertical and longitudinal component data, which are selected independently, throughout the upper mantle, and from transverse component data in the uppermost 250 km (where Love waves are most sensitive) indicates that the features obtained in the Q model are stable up to $smax \sim 8$. This confirms the validity of our selection procedures in dealing with unwanted perturbing effects on the amplitudes.

23. Montagner, J.P. and T. Tanimoto, *J. Geophys. Res.* **96**, 20,337 (1991).

24. Ekström, G. and A. M. Dziewonski, *Nature*, **394**, 168 (1997).

25. The transverse component data provide constraints on the topmost 200 km of the mantle, while Z and L components (and in particular higher mode waveforms) provide resolution in the upper mantle transition zone. Our confidence in the stability of the Q patterns derives from the comparison of models obtained independently using Z, L, or T data, as well as bootstrapping and resolution experiments. The resolution experiments confirm our ability to distinguish structures in the uppermost 250km from those at larger depth, whereas inversions using different components confirm that contamination by elastic effects does not dominate the observed patterns. Gung and Romanowicz, in preparation.

26. Durek, J.J. and G. Ekström, *Bull. Seism. Soc. Am.* **86**, 144 (1996).

27. Babuśka, V., J-P. Montagner, J. Plomerova and N. Girardin, *Pure Appl.Geophys.* **151**, 257 (1998).

28. Jung, H. Y. and S. I. Karato, Water-induced fabric transitions in olivine, Science, 293, 1460-1463 (2001).

29. Montagner, J. P. and L. Guillot, in *Problems in Geophysics for the New Millenium*, E. Boschi et al. Eds, 218 (2000).

30. The existence of a low viscosity channel under the lithosphere has been recognized

for some time from modelling of glacial rebound as well as joint modelling of gravity and seismological data (e.g. Davies and Richards *J. Geolog.* **100**, 151 (1992); Mitrovica, J. X. amd A. M. Forte *J. Geophys. Res.* **102**, 2751 (1997)); it has been suggested recently that it could be as low as $10^{18}$ Pas under the Pacific ocean (e.g. Pollitz, F.,R. Bürgmann and B. Romanowicz *Science* **280**, 1245 (1998)).

31. The significant supply of upwelling heat over a wider area under Africa may explain the anomalous heat flow in south Africa (A. Nyblade and S. Robinson, *Geophys. Res. Lett.* **21**, 765 (1994)) and the anomalous topography in the African Superswell (C. Lithgow-Bertelloni and P. G. Silver, *Nature* **395**, 269 (1998)), and the south Pacific (McNutt, M. *Rev. Geophys.* **36**, 211 (1998)).

32. Wolfe, C., I. T. Bjarnason, J. VanDecar and S. C. Solomon, *Nature* **386**, 328; Foulger, G. and D. G. Pearson, *Geophys. J.*, **145**, F1 (2001).

33. Hart, S. R., E. H. Hauri, L. A. Oschmann, and J. A. Whitehead, *Science* **256**, 517 (1995).

34. Castillo, P., *Nature* **336**, 667 (1988).

35. Burke, K. *EOS Trans Am. Geophys. Union* **82**, F1134 (2001).

36. Morgan, W. J., *Nature* **230**, 42 (1971)

37. Sleep, N., Hotspots and mantle plumes: some phenomenology, J. Geophys. Res., 95, 6715 (1990); Davies, J., *J. Geophys. Res.* **93**, 10,467 (1988).

**Figure Captions**

**Fig. 1**. Maps of lateral variations in Q at representative depths in the upper mantle, obtained by joint inversion of 3 component waveform data (model $QRLW8$ *(25)*. The maximum in the color scale is indicated in parenthesis for each map, with blue and red corresponding to high and low Q, respectively. Black dots are hotspots *(7)* and the global plate boundary system is green, emphasizing the changing Q pattern as depth increases. Note that the two low Q minima in the transition zone appear to be connected through south America, following the trail of southern hotspots. Temperature contrasts at the center of the low Q regions in the transition zone could be several hundred degrees, however amplitudes of lateral variations in Q are not well constrained.

**Fig. 2**. Comparison of the degree 2 distribution in Q in the upper mantle transition zone (depth of 500 km), for model $QRLW8$, with the corresponding distribution in $SH$ and $SV$ velocity, as well as with $SH$ velocity at 2600 km. The $SH$ model is $SAW24B16$*(2)*. The $SV$ model, $SAW16BV$ was derived in the course of the present study (Gung and Romanowicz, in preparation). There is no corresponding $SV$ velocity model in the deepest mantle, as the sampling in $SV$ at those depths is poorer than for $SH$. Note that the velocity models in the transition zone correlate better with slabs than with superplumes.

**Fig. 3**. Top panels: Map views of model $QRLW8$ centered on the low Q minima in the Pacific (a) and Africa (b). Bottom panels: Depth cross-sections along profiles indicated in the top panels showing, for each profile (top to bottom), $V_{SH} - V_{SV}$ distribution in the upper mantle, Q distribution in the upper mantle, and $V_{SH}$ distribution in the lower mantle. The upper mantle cross-sections start at 80km depth because our Q modeling does not have resolution above that depth. Mid-ocean ridge positions are indicated by arrows. Note the position of the low Q regions in the transition zone above the lowermost mantle low velocity minima. Zones of positive $V_{SH} - V_{SV}$ in the uppermost mantle (blue)

correspond to zones where the low $Q$ regions are shifted horizontally with respect to their transition zone location. This shift in $Q$ is well resolved, as indicated by synthetic tests. Although lower than average velocities are generally present above the superplumes in the lower mantle, they are not well defined above 2000km depth. Their contorted shape is intriguing, but it is not clear whether it is real or an artifact of limited resolution in this depth range. Ridges are generally shallow features (e.g. at S,N and B), except in the south Atlantic (at M) where the ridge is also connected to the depper low Q zone under south America. Note the negative $V_{SH} - V_{SV}$ at shallow depth under the African cratons, consistent with other studies *27*.

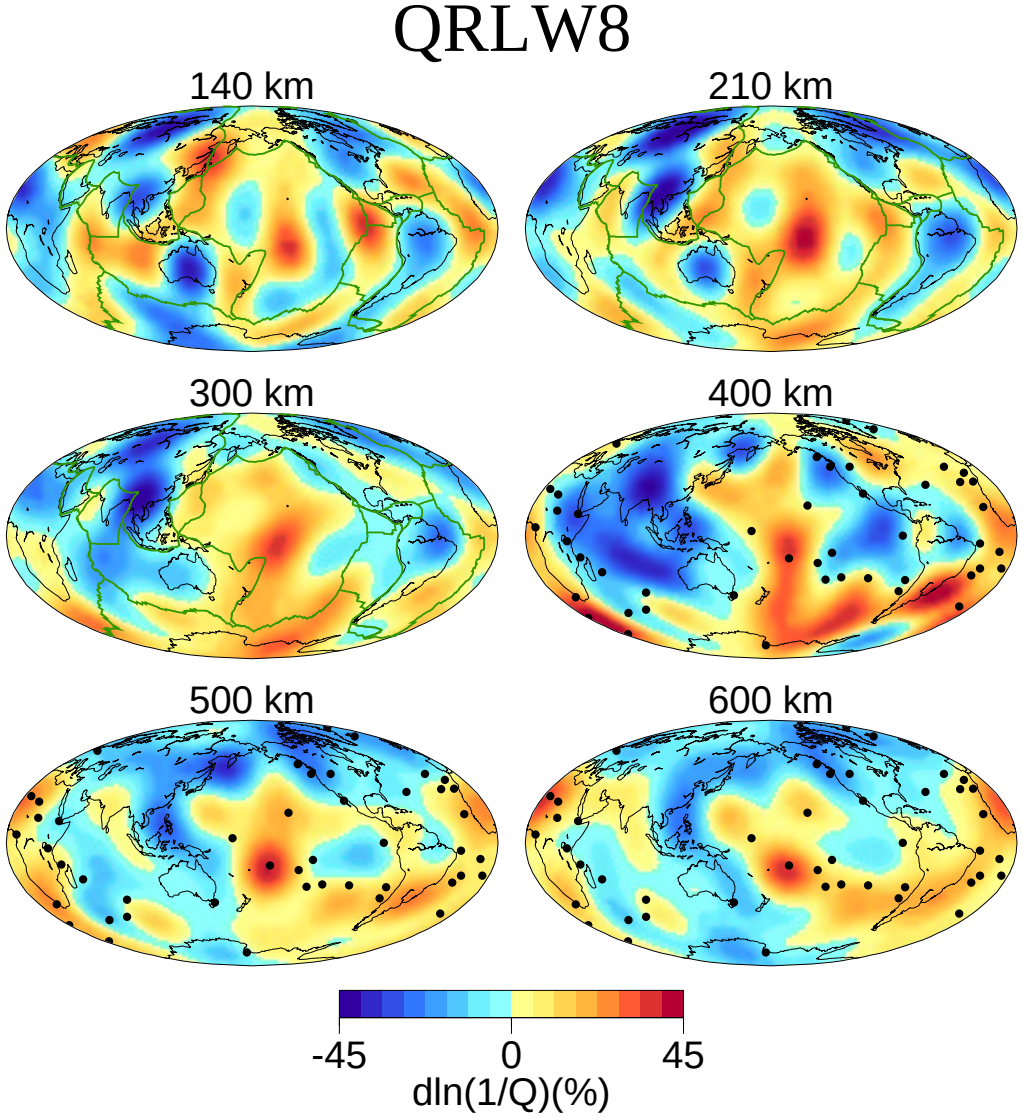


Figure 1:

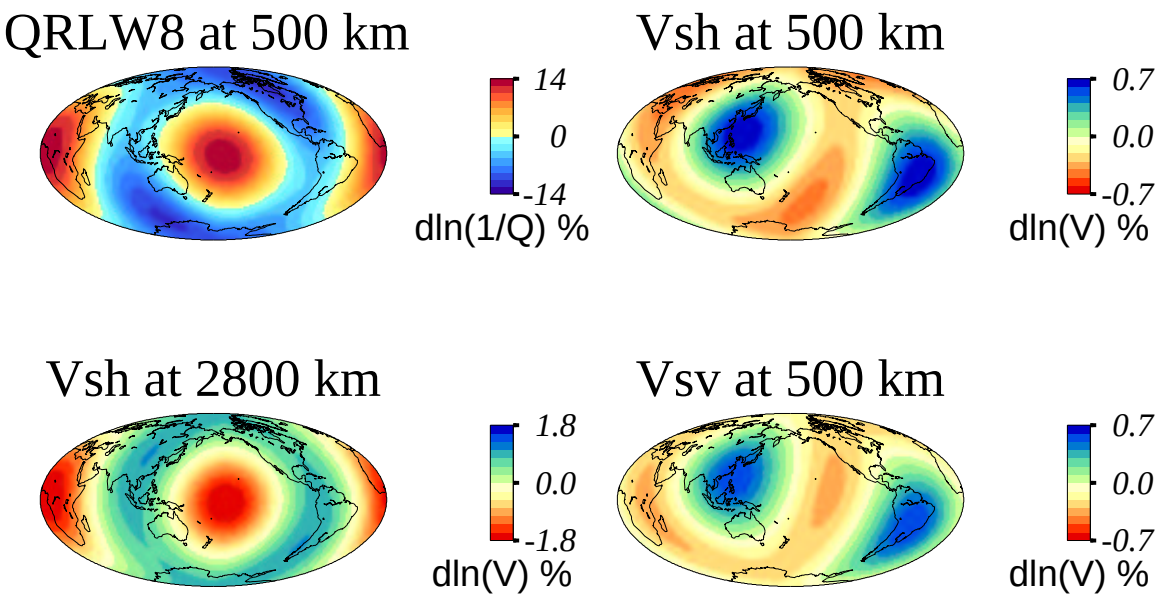
QRLW8 at 500 km
14
0
-14
dln(1/Q) %
Vsh at 500 km
0.7
0.0
-0.7
dln(V) %
Vsh at 2800 km
1.8
0.0
-1.8
dln(V) %
Vsv at 500 km
0.7
0.0
-0.7
dln(V) %

Figure 2:

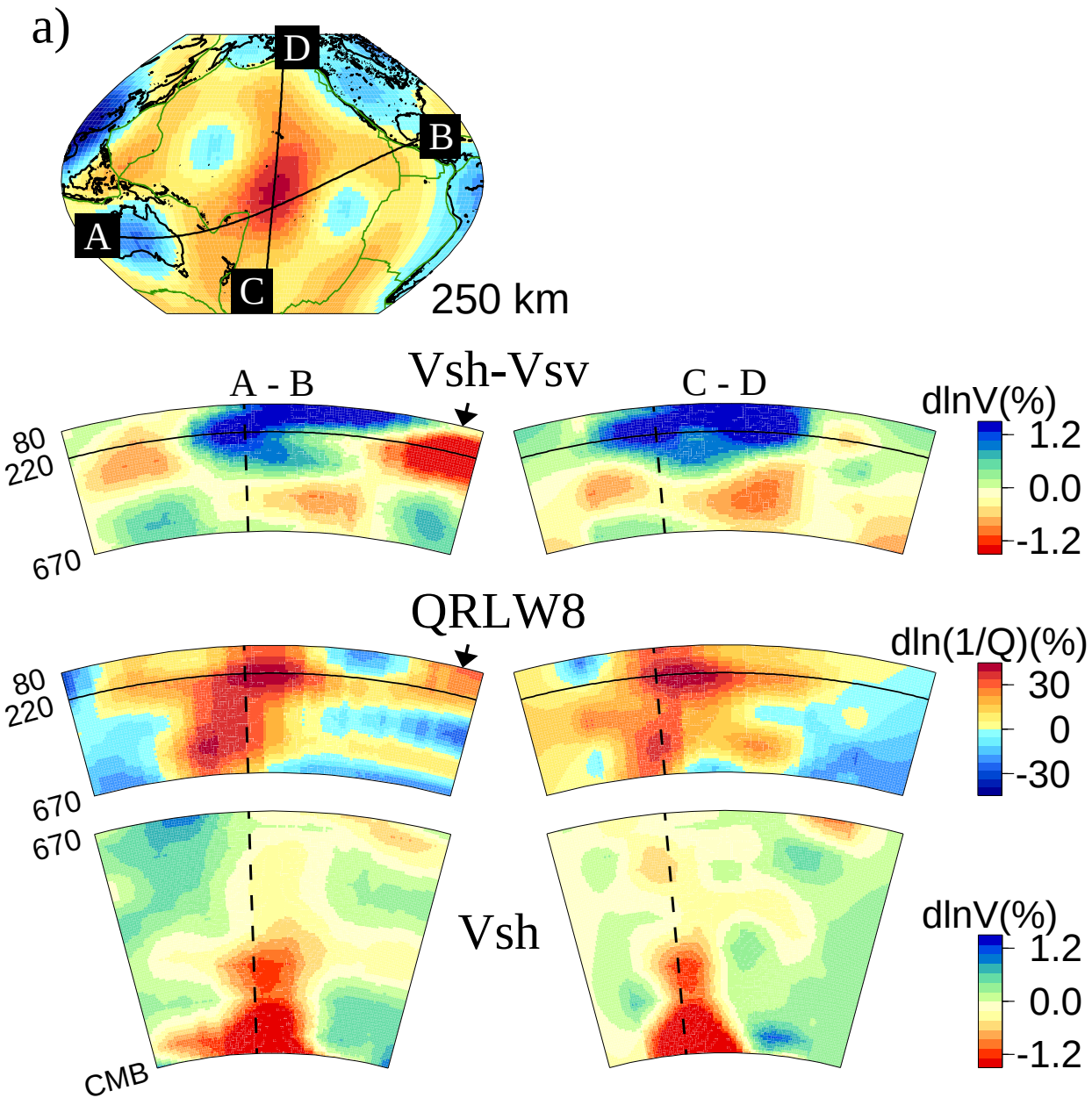
a)
D
B
A
C
250 km
Vsh-Vsv
A - B
C - D
dlnV(%)
1.2
0.0
-1.2
80
220
670
QRLW8
dln(1/Q)(%)
30
0
-30
670
Vsh
dlnV(%)
1.2
0.0
-1.2
CMB

Figure 3: a

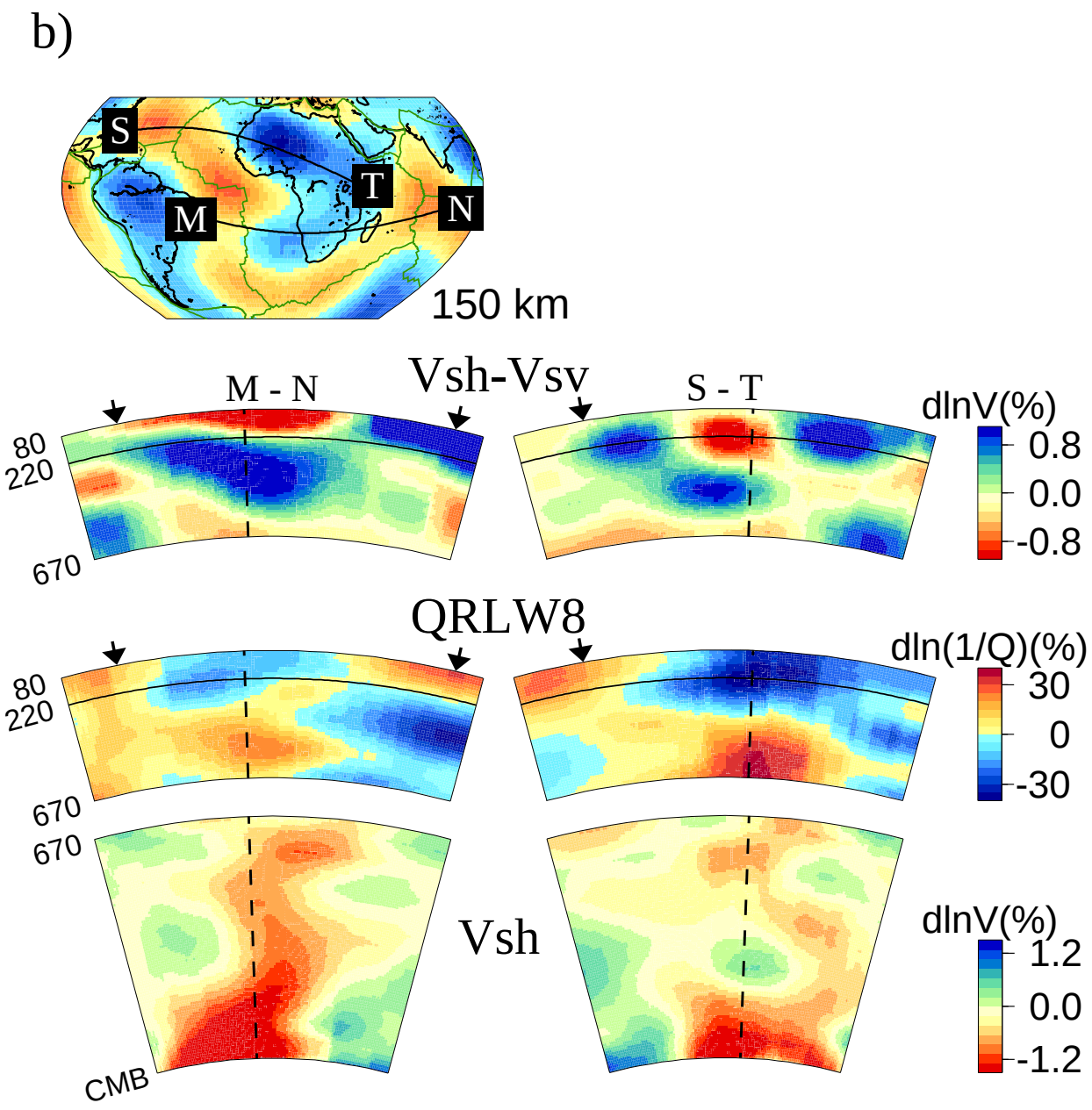
b)
S
T
M
N
150 km
Vsh-Vsv
M - N
S - T
dlnV(%)
0.8
0.0
-0.8
80
220
670
QRLW8
dln(1/Q)(%)
30
0
-30
670
Vsh
dlnV(%)
1.2
0.0
-1.2
CMB

Figure 4: b